Protein kinase A activity is regulated by actomyosin contractility during cell migration and is required for durotaxis

Andrew J. McKenzie[a,b,†], Kathryn V. Svec[a,b,†], Tamara F. Williams[a,b], and Alan K. Howe[a,b,c,*]
[a]Department of Pharmacology, [b]University of Vermont Cancer Center, and [c]Department of Molecular Physiology and Biophysics, University of Vermont, Burlington, VT 05405

ABSTRACT **Dynamic subcellular regulation of protein kinase A (PKA) activity is important for the motile behavior of many cell types, yet the mechanisms governing PKA activity during cell migration remain largely unknown. The motility of SKOV-3 epithelial ovarian cancer (EOC) cells has been shown to be dependent both on localized PKA activity and, more recently, on mechanical reciprocity between cellular tension and extracellular matrix rigidity. Here, we investigated the possibility that PKA is regulated by mechanical signaling during migration. We find that localized PKA activity in migrating cells rapidly decreases upon inhibition of actomyosin contractility (specifically, of myosin ATPase, Rho kinase, or myosin light-chain kinase activity). Moreover, PKA activity is spatially and temporally correlated with cellular traction forces in migrating cells. Additionally, PKA is rapidly and locally activated by mechanical stretch in an actomyosin contractility-dependent manner. Finally, inhibition of PKA activity inhibits mechanically guided migration, also known as durotaxis. These observations establish PKA as a locally regulated effector of cellular mechanotransduction and as a regulator of mechanically guided cell migration.**

Monitoring Editor
Yu-li Wang
Carnegie Mellon University

Received: Mar 1, 2019
Revised: Oct 24, 2019
Accepted: Nov 7, 2019

INTRODUCTION

Cells sense, respond to, and contribute to the mechanical properties of the extracellular matrix (ECM) by exerting actomyosin-dependent contractile force on integrin-based adhesive contacts and sensing countertension through mechanochemical systems (Bershadsky *et al.*, 2003; Janmey and McCulloch, 2007; Schwartz, 2010; Levayer and Lecuit, 2012; Schiller and Fassler, 2013; Ringer *et al.*, 2017; Weinberg *et al.*, 2017). Integrin engagement and clustering initiate the generation of cellular forces through actomyosin contractility (Chrzanowska-Wodnicka and Burridge, 1996; Choquet *et al.*, 1997; Balaban *et al.*, 2001), which in turn promotes maturation and strengthening of adhesive contacts, thereby providing countertension to the force of protrusive actin polymerization within leading-edge lamellipodia and large-scale contractility to pull the cell body in the direction of migration (Riveline *et al.*, 2001; Parker *et al.*, 2002; Prager-Khoutorsky *et al.*, 2011; Wolfenson *et al.*, 2011; Plotnikov *et al.*, 2012; Plotnikov and Waterman, 2013; Roca-Cusachs *et al.*, 2013; Lintz *et al.*, 2017). The distribution of contractile forces within a migrating cell generates subcellular areas with varying degrees of intracellular tension, countered both by internal cytoskeletal scaffolds and by matrix adhesions (Ingber, 1997; Schwartz, 2010). Intracellular contractile forces regulate myriad aspects of cell migration (Vicente-Manzanares *et al.*, 2011; Levayer and Lecuit, 2012; Plotnikov *et al.*, 2012; Pasapera *et al.*, 2015; Schiffhauer and Robinson, 2017), and during the migration of many cell types, traction force tends to be highest within the leading edge, often within the lamella just behind actively protruding lamellipodia (Bereiter-Hahn and Luers, 1998; Dembo and Wang, 1999; Lo *et al.*, 2000; Beningo *et al.*, 2001; McKenzie *et al.*, 2018).

cAMP-dependent protein kinase (PKA) is an important regulator of myriad targets involved in cell migration and cytoskeletal

This article was published online ahead of print in MBoC in Press (http://www.molbiolcell.org/cgi/doi/10.1091/mbc.E19-03-0131) on November 13, 2019.

†These authors contributed equally to this work.

*Address correspondence to: Alan K. Howe (Alan.Howe@med.uvm.edu).

Abbreviations used: AKAP, A-kinase anchoring protein; Blebb, blebbistatin; CFP, cyan fluorescent protein; EOC, epithelial ovarian cancer; FRET, Förster resonance energy transfer; FSK, forskolin; IBMX, isobutyl methylxanthine; ICQ, intensity correlation quotient; LynAKAR4, Lyn-modified A-kinase activity reporter 4; mCh-PKI, mCherry–protein kinase inhibitor; PKA, cAMP-dependent protein kinase; pmAKAR3, plasma membrane A-kinase activity reporter 3; Pxn, paxillin; SH2, Src-homology 2; TFM, traction force microscopy; YFP, yellow fluorescent protein.

dynamics (Howe, 2004, 2011), and localized activation of PKA signaling, facilitated by A-kinase anchoring proteins (AKAPs), is necessary for the motile behavior of numerous cell types (Howe *et al.*, 2005; Lim *et al.*, 2007, 2008; Paulucci-Holthauzen *et al.*, 2009; Zhang *et al.*, 2010; McKenzie *et al.*, 2011; Tkachenko *et al.*, 2011; Takahashi *et al.*, 2013; Deming *et al.*, 2015; Sinha *et al.*, 2015). However, the mechanisms controlling PKA activation during migration remain unclear.

Previously, we showed that efficient migration of SKOV-3 human ovarian cancer cells requires localized PKA activity within the leading edge (McKenzie *et al.*, 2011). More recently, we demonstrated that SKOV-3 cell migration is also governed by the mechanical microenvironment; specifically, that cell contractility and migration positively correlate with ECM stiffness and that directional increases in ECM tension promote SKOV-3 cell durotaxis (McKenzie *et al.*, 2018). In the present work, we explore the possibility that localized PKA activity in migrating cells might be regulated by mechanical signaling and cell–matrix tension.

RESULTS

Protein kinase is activated at the leading edge during cell migration but not at the periphery during cell spreading

In an attempt to facilitate the investigation of the regulation of PKA within the leading edges of migrating cells, we performed live-cell Förster resonance energy transfer (FRET) microscopy using pmAKAR3, a genetically encoded PKA biosensor consisting of a sensor cassette (a PKA-specific substrate domain and a flanking phosphoamino acid–binding FHA1 domain) located between ECFP and an EYFP variant (cpV-E172), and a C-terminal CAAX box (derived from K-Ras) for targeting to the plasma membrane (Allen and Zhang, 2006). PKA-mediated phosphorylation of the pmAKAR3 substrate domain promotes intramolecular binding by the FHA1 domain, juxtaposition of the fluorophores, and increased FRET. Mutation of the PKA phosphorylation site in pmAKAR3 from Thr to Ala (pmAKAR3^{TA}) ablates the baseline FRET signal and renders the biosensor unresponsive to pharmacological elevation of cAMP by treatment with forskolin and IBMX (to activate adenylyl cyclase and inhibit phosphodiesterases, respectively; Supplemental Figure S1A). Importantly, it is this biosensor that has been used and characterized most extensively to describe and investigate localized PKA activity in migrating cells (Lim *et al.*, 2008; Paulucci-Holthauzen *et al.*, 2009; McKenzie *et al.*, 2011; Tkachenko *et al.*, 2011). We first used pmAKAR3 to compare the PKA activity in the leading edges of migrating SKOV-3 cells and in the peripheries of spreading SKOV-3 cells, shortly after plating onto fibronectin-coated surfaces, as this periphery is often used as a model for the migratory leading edge (e.g., Giannone *et al.*, 2007). Consistent with prior reports (McKenzie *et al.*, 2011), robust and dynamic PKA activity was seen within the leading edge of migrating cells (Figure 1, B and C; Supplemental Movie S1). No FRET signal was observed in cells expressing the phosphoresistant pmAKAR3^{TA} mutant biosensor (Supplemental Figure S1B; Supplemental Movie S2), confirming that the leading-edge signal from the wild-type sensor is indeed due to biosensor phosphorylation. In contrast to the robust activity at the leading edge, PKA activity in the peripheries of spreading cells was very low (Figure 1, A and C; Supplemental Movie S1). This was somewhat surprising, given that prior investigations have reported, using biochemical methods, some degree of activation of PKA early upon integrin engagement and during cell spreading (Whittard and Akiyama, 2001; Howe *et al.*, 2002). It is important to reiterate, here, that the pmAKAR3 biosensor used throughout this study (and others; Lim *et al.*, 2008; Paulucci-Holthauzen *et al.*, 2009; McKenzie *et al.*, 2011; Tkachenko *et al.*, 2011) is targeted to the plasma membrane and thus reports only membrane-proximal events, and therefore might not detect other pools of PKA that might be activated during spreading. That notwithstanding, the exceedingly low PKA peripheral activity suggests that spreading cells are not a suitable experimental system for studying regulation of PKA within the leading edge.

Leading-edge protein kinase activity events are spatially and temporally distinct from sites of focal adhesion formation

Over the course of additional experimentation and optimization of conditions for visualizing localized PKA activity during migration, we noticed that activation of PKA at the leading edge was common to many modes of migration under a variety of culture conditions; for example, signaling events were seen in the presence or absence of serum, before and after serum starvation, and with and without supplemental growth factor, albeit with differences in signaling event morphology and kinetics (Supplemental Movie S3). This suggested that, rather than being instigated by soluble cues from culture media, the mechanisms governing localized PKA activity during migration might be governed by something intrinsic to cells as they move.

One process common to most, if not all, modes of migration is the engagement of integrins by the ECM and the subsequent formation of adhesive complexes such as focal contacts and focal adhesions (Mostafavi-Pour *et al.*, 2003). Importantly, engagement of integrins has also been implicated in activation of PKA (O'Connor and Mercurio, 2001; Whittard and Akiyama, 2001; Goldmann, 2002; Howe *et al.*, 2002, 2005; Howe, 2004; Alenghat *et al.*, 2009; Tkachenko *et al.*, 2011). We therefore investigated whether there were any spatiotemporal links between leading-edge PKA signaling events and the formation of focal adhesion. For this, we imaged cells coexpressing pmAKAR3 and mCherry–paxillin to visualize PKA activity and focal adhesion dynamics, respectively. Paxillin was used as a marker of focal adhesions because it recruits to focal adhesions early in the maturation process and remains through the entirety of the adhesion lifetime (Zaidel-Bar *et al.*, 2003). Visual assessment of numerous images suggested no close or obvious spatial correlation between leading-edge PKA events and paxillin-containing focal adhesions (Figure 2A). To further assess any spatiotemporal correlation between focal adhesion dynamics and PKA activity, leading-edge focal adhesions were tracked over time and an interrogation region of interest (ROI) 50% larger than the area of the adhesion was used to track pmAKAR3 FRET ratios under the same cellular regions (Figure 2B). Paxillin displayed full adhesion life cycles including assembly, peak, and disassembly phases (Figure 2C, red line), while PKA activity showed little, if any, variation in the same regions. Additionally, ROIs were placed around areas of dynamic leading-edge PKA activity events and used to measure corresponding mCherry–paxillin intensities (Figure 2D). Interestingly, there was no apparent covariation between the intensity of mCherry–paxillin and peak PKA activity events (Figure 2E). Similar results were seen when mCherry–FAK was used as a distinct focal adhesion marker (Supplemental Figure S2). Integrin-containing complexes are known to generate myriad signals—most notably, a local increase in tyrosine phosphorylation and phosphotyrosine-dependent protein–protein interactions (Humphries *et al.*, 2019). Thus, to ensure that the lack of coincidence between PKA events and focal adhesion dynamics was not due to an inability to detect adhesion-associated signaling events, cells were cotransfected with mCherry–paxillin and YFP-dSH2 (Kirchner *et al.*, 2003), a phosphotyrosine reporter comprising yellow fluorescent protein fused to two tandem Src SH2 domains

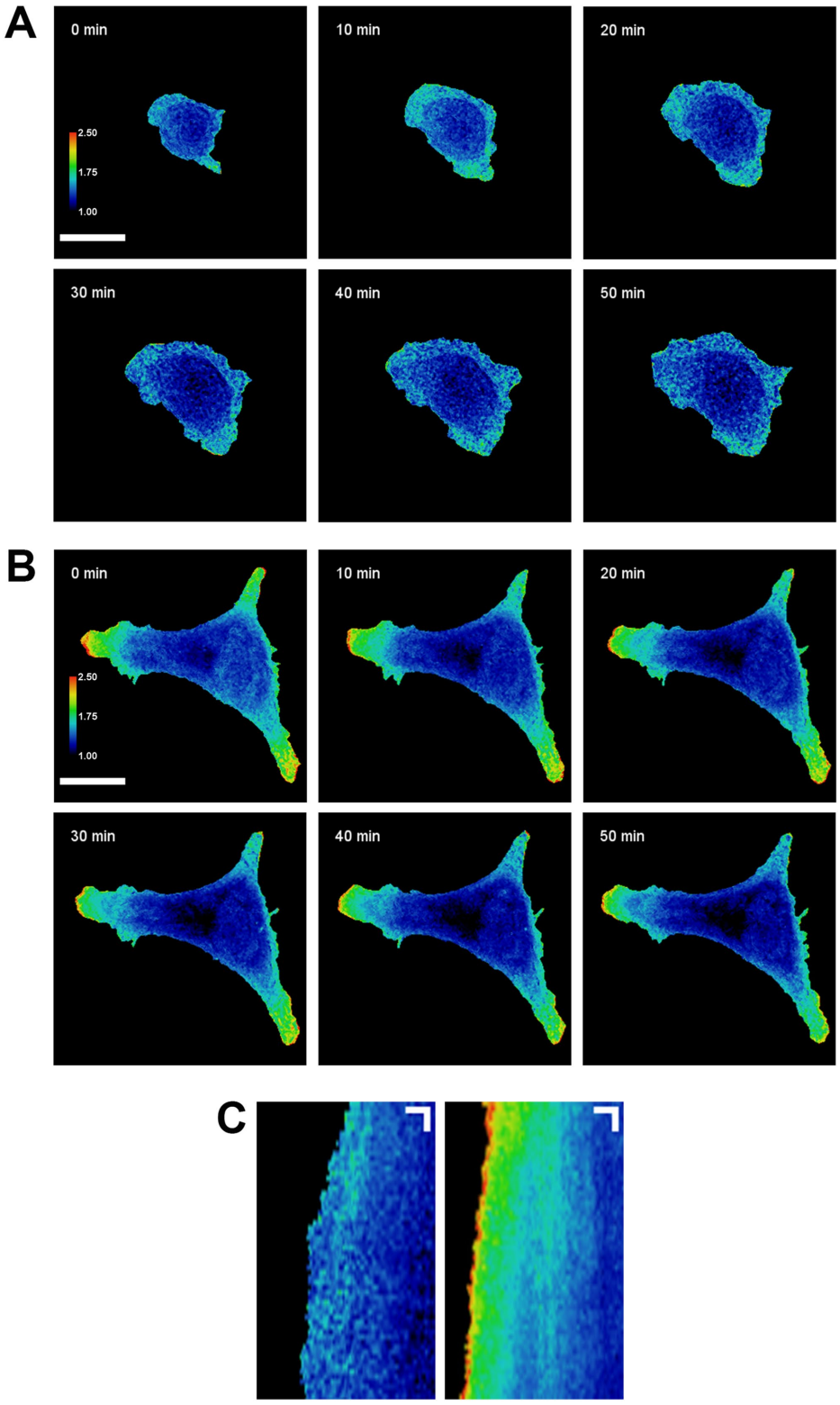

FIGURE 1: PKA activity is increased at the leading edge of migrating cells but not at the periphery of spreading cells. SKOV-3 cells expressing pmAKAR3 were plated onto fibronectin-coated glass coverslips and imaged via FRET microscopy10 min (A) or 4 h (B) after plating. Representative pseudocolored FRET/CFP images of spreading (A) and migrating (B) cells are shown (bar = 25 μm). FRET ratios of each image are scaled from 1.0 to 2.5 (cool to warm color). (C) A linescan analysis of the change in centroid-to-front FRET ratio was performed on the spreading (left) and migrating (right) cells from A and B. Kymographs represent the FRET ratio along the linescans shown in Supplemental Movie S1 over the course of 1 h. Images were acquired every 60 s. Kymograph scale bars represent 5 μm on the *X* axis and 5 min on the *Y* axis.

that bind phosphotyrosine. As expected, we saw strong covariation of paxillin intensity and the intensity of YFP-dSH2 during the assembly, peak, and disassembly of focal adhesions (Figure 2F). Quantification of Pearson's correlation coefficients showed a strong positive correlation between mCherry–paxillin and YFP-dSH2, but no correlation between pmAKAR3 FRET ratios and mCherry–paxillin (Figure 2G). While we cannot rule out a role for small and/or transient focal complexes that are below our threshold of detection, these results demonstrate that leading-edge PKA dynamics is not spatiotemporally correlated with the onset, maturation, or dissolution of mature focal adhesions in migrating cells. This suggests that leading-edge PKA activity is regulated through a mechanism dependent on, but downstream of and spatially removed from, integrin-mediated focal adhesion formation.

In addition to spanning the plasma membrane, integrins and their dependent adhesion complexes can both regulate and be regulated by membrane order and lipid raft dynamics in complex ways (Leitinger and Hogg, 2002; Gagnoux-Palacios *et al.*, 2003; Del Pozo, 2004; del Pozo *et al.*, 2004, 2005; Fabbri *et al.*, 2005; Gaus *et al.*, 2006; Vassilieva *et al.*, 2008; Norambuena and Schwartz, 2011; Wang *et al.*, 2013; Head *et al.*, 2014; Sun *et al.*, 2016). Importantly, PKA also has distinct functions in lipid rafts (Golub and Caroni, 2005; Ruppelt *et al.*, 2007; Delint-Ramirez *et al.*, 2011; Raslan and Naseem, 2015), and work using distinctly targeted PKA biosensors has demonstrated differential regulation of PKA in bulk plasma membrane as compared with lipid rafts (Depry *et al.*, 2011). Therefore, to determine whether a spatiotemporal correlation might exist between adhesion dynamics and leading-edge PKA activity in a distinct membrane microdomain, we visualized PKA dynamics in migrating cells using the lipid raft–targeted biosensor LynAKAR4 (Depry *et al.*, 2011). Similarly to the activity seen with pmAKAR3, dynamic PKA activity was also observed in the leading edges of LynAKA4-expresing cells, albeit with discernibly distinct patterns and dynamics (Supplemental Figure S3A; Supplemental Movie S4). Notably, these distinct raft-associated PKA activity events also did

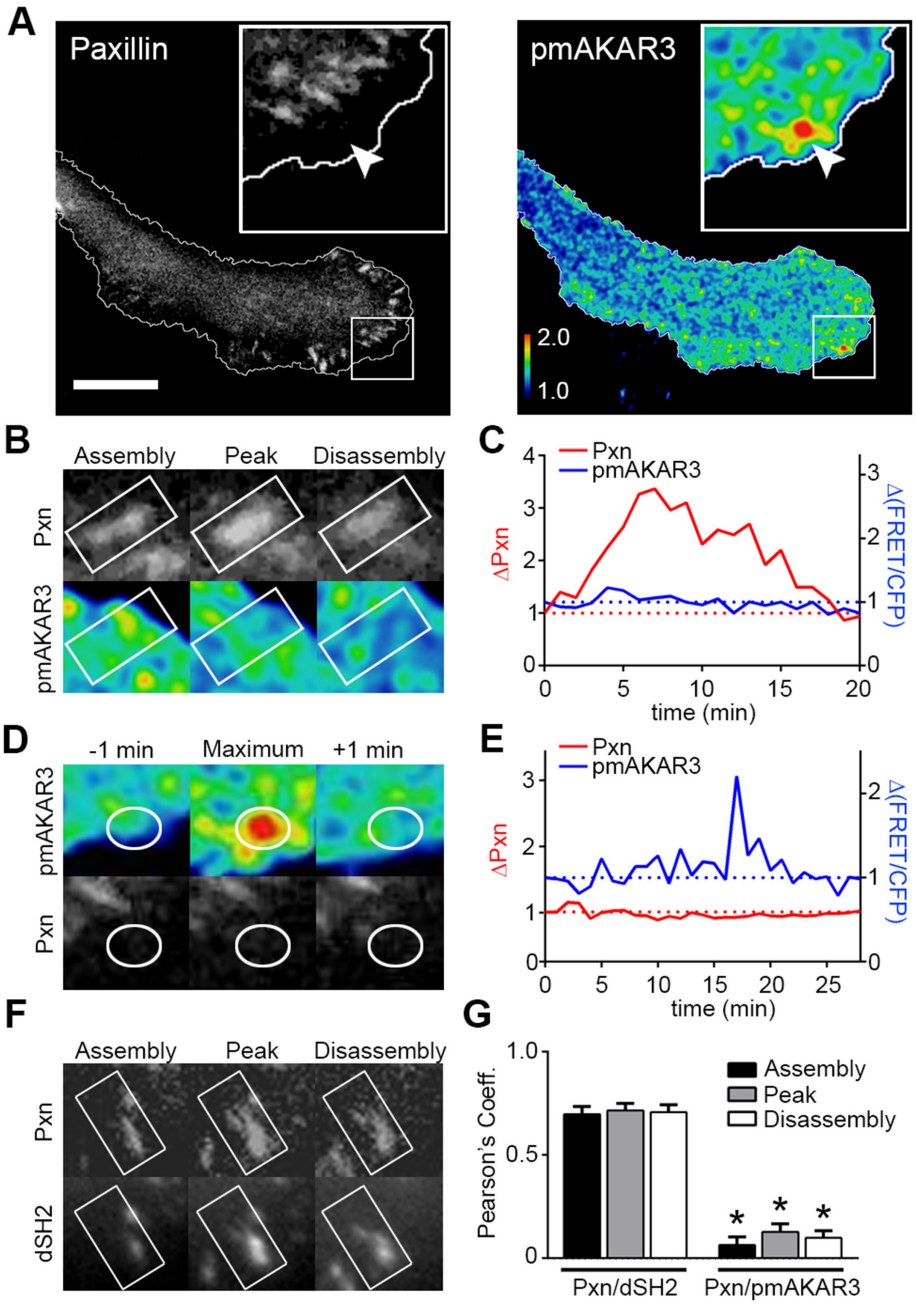

FIGURE 2: Leading-edge PKA activity does not correlate with focal adhesion dynamics. (A) Migrating SKOV-3 cells coexpressing pmAKAR3 and mCherry–paxillin were plated onto fibronectin-coated imaging dishes, and representative near-simultaneous paxillin (Pxn) and pseudocolored FRET/CFP (pmAKAR3) images from live-cell microscopy experiments are shown. Arrow indicates location of peak FRET/CFP signal and corresponding location on mCherry–paxillin image. The leading edge is magnified in the insets, shown with cell outlines plotted for reference (bar = 10 μm). (B) Images of a single paxillin-containing focal adhesion during assembly, peak, and disassembly (top) with overlapping pseudocolored FRET/CFP (bottom) are shown. (C) The changes in either paxillin fluorescence intensity or FRET ratios were plotted over time. (D) Images of dynamic PKA activity and the corresponding paxillin images are shown with ROI plotted as a reference. (E) The changes in either FRET ratios or paxillin fluorescence intensity were plotted over time. (F) YFP-dSH2 and paxillin intensities were tracked over time during focal adhesion assembly, peak, and disassembly. (G) Pearson's coefficients of the covariance of paxillin with either YFP-dSH2 (Pxn/dSH2) or pmAKAR3 (Pxn/pmAKAR3) during focal adhesion assembly, peak, and disassembly are shown as mean ± SEM (Pxn/dSH2, $n = 10$; Pxn/pmAKAR3, $n = 13$; * $p < 0.001$ for each phase of focal adhesion lifetime).

not correlate closely with focal adhesion assembly dynamics in space or time (Supplemental Figure S3B), confirming the assertion that PKA activity in leading-edge membranes is regulated through a mechanism that is downstream of and/or spatially separated from integrin-mediated focal adhesion formation.

Leading-edge protein kinase activity is regulated by actomyosin contractility

In further consideration of what might regulate PKA activity during migration, we began to consider a cellular characteristic that is dependent on integrin-mediated adhesion, intrinsic to many cells across many modes of migration, and not typically associated with cell spreading—namely, actomyosin-dependent cellular contractility (Bershadsky *et al.*, 2003; Wakatsuki *et al.*, 2003; Zhang *et al.*, 2008; Wolfenson *et al.*, 2011; Plotnikov *et al.*, 2012). Intracellular contractile forces regulate diverse aspects of signaling and cytoskeletal dynamics during cell migration (Vicente-Manzanares *et al.*, 2011; Levayer and Lecuit, 2012; Plotnikov *et al.*, 2012; Pasapera *et al.*, 2015; Schiffhauer and Robinson, 2017) and, importantly, these forces tend to be highest within the leading edge (Bereiter-Hahn and Luers, 1998; Dembo and Wang, 1999; Lo *et al.*, 2000; Beningo *et al.*, 2001; McKenzie *et al.*, 2018), placing them in the correct subcellular location to affect PKA activity.

To investigate whether cellular contractility affected PKA dynamics, we imaged PKA activity in live cells before and after addition of blebbistatin, an inhibitor of the myosin II-ATPase. Upon addition of blebbistatin, localized and dynamic activity of PKA at the leading edge rapidly and significantly diminished (Figure 3, A and B; Supplemental Movie S5), suggesting that this localized activity is dependent on actomyosin contractility. Exposure of blebbistatin to blue light (≤488 nm), however, can inactivate the compound and generate cytotoxic free radicals (Kolega, 2004; Sakamoto *et al.*, 2005), although attenuation of light intensity and rapid diffusion of "fresh" drug from the media bath into cells often allow its utility in live-cell imaging experiments using blue light excitation (Hotulainen and Lappalainen, 2006; Burnette *et al.*, 2008; Aratyn-Schaus and Gardel, 2010; Myers *et al.*, 2011). Nonetheless, to ensure that blebbistatin-mediated inhibition of leading-edge PKA activity was due to inhibition of contractility and not cytotoxicity, we repeated this experiment with other contractility

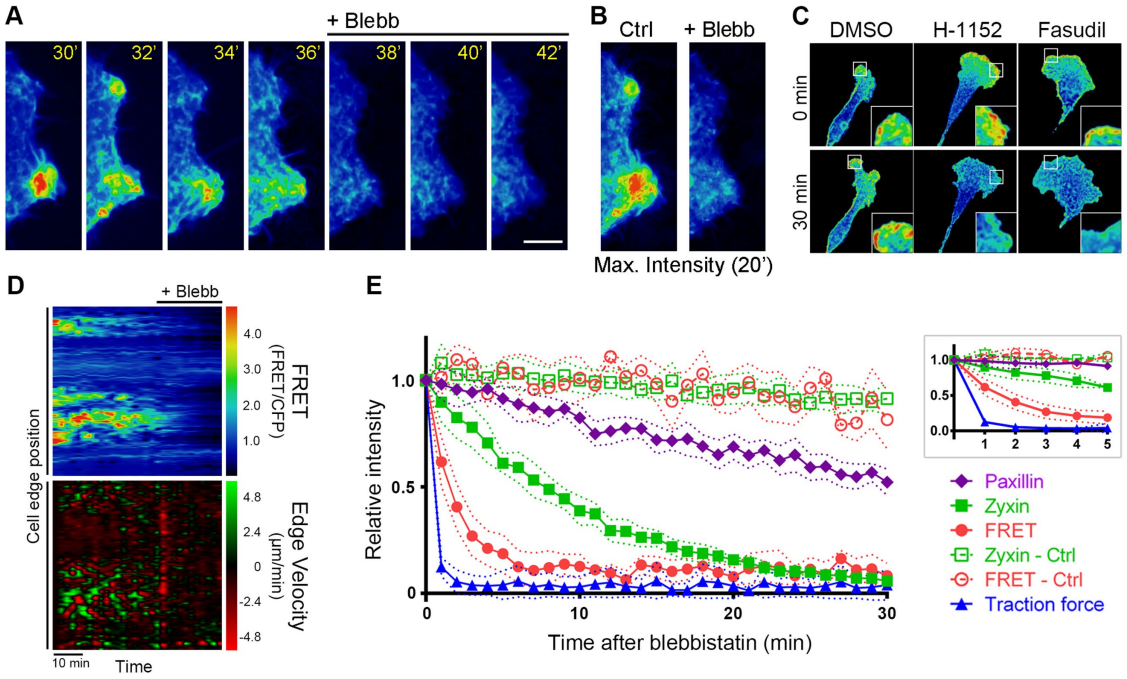

FIGURE 3: Actomyosin contractility regulates leading-edge velocity and PKA activity. (A) A migrating SKOV-3 cell expressing pmAKAR3 was plated on a fibronectin-coated glass-bottomed imaging dish and monitored by live-cell microscopy before and after treatment with 25 μM blebbistatin (Blebb). Representative pseudocolored FRET/CFP images (corresponding to the boxed region in Supplemental Movie S3) are shown. (B) A maximum-intensity projection of cumulative PKA activity in 10 images (2 min apart) before and after treatment with blebbistatin. (C) Representative images of pmAKAR3-expressing SKOV-3 cells migrating on fibronectin-coated dishes before (0 min) and 30 min after treatment with 0.1% vol/vol dimethyl sulfoxide (DMSO), 1 μM H-1152, or 10 μM fasudil. The leading edge is magnified in the insets (scale bar = 10 μm). (D) QuimP11 software (Bosgraaf and Van Haastert, 2010) was used to generate maps of PKA activity (top) and edge velocity (bottom) within a 10-μm band along the leading edge before and after treatment with blebbistatin (Blebb). (E) SKOV-3 cells expressing mCherry–paxillin, mCherry–zyxin, or pmAKAR3 (FRET) migrating on fibronectin-coated glass dishes, or cells plated on 125 kPa fluorescent nanosphere-functionalized hydrogels (traction force) were treated with 25 μM blebbistatin (or with 0.1% vol/vol DMSO; Ctrl) at time = 0. Capturing images every 60 s, the fluorescence intensity of paxillin or zyxin within focal adhesions, PKA activity (via the pmAKAR FRET signal), or traction force was measured, normalized to values at $t = 0$, and plotted. The graph depicts mean values ± SEM ($n_{\text{paxillin-Blebb}} = 211$ adhesions from seven cells; $n_{\text{zyxin-Blebb}} = 156$ adhesions from five cells; $n_{\text{FRET}} = 30$ linescans from six cells; $n_{\text{zyxin-Ctrl}} = 125$ adhesions from five cells; $n_{\text{FRET-Ctrl}} = 35$ linescans from seven cells; $n_{\text{traction force}}$ = average traction from six cells). The inset shows the first 5 min of the time course at higher resolution; these data were used to calculate the one-phase half-life ($t_{½}$) or apparent $t_{½}$ decay values for each signal, using GraphPad Prism.

inhibitors. Initial attempts at imaging pmAKAR3-expressing cells before and after addition of para-aminoblebbistatin, a nontoxic blebbistatin derivative that is supposedly nonfluorescent (Varkuti *et al.*, 2016), gave uninterpretable results due to significant yellow fluorescence of the drug inside cells—an observation confirmed in nontransfected cells (Supplemental Figure S4). We therefore employed compounds that are devoid of phototoxicity and optical artefacts and inhibit actomyosin contractility (Supplemental Figure S5) through distinct mechanisms; specifically, through inhibition of Rho-kinase (using H-1152, Fasudil/HA-1077, or Y-27632) or myosin light-chain kinase (using ML-7), both of which contribute to the phosphorylation and activation of the myosin light chain (MLC) of myosin II to promote contractility (Amano *et al.*, 1996; Totsukawa *et al.*, 2000). Treatment of migrating, pmAKAR3-expressing cells with each of these compounds lead to a rapid and significant decrease in leading-edge PKA activity (Figure 3C; Supplemental Movie S6; Supplemental Figure S6). Leading-edge PKA activity visualized by LynAKAR4 showed a similar dramatic reduction upon inhibition of Rho-kinase by Y-27632 (Supplemental Figure 3C), further supporting the observation that leading-edge PKA activity is dependent on actomyosin contractility.

Inhibition of actomyosin contractility is associated with discrete morphological effects, including cessation of leading-edge dynamics and eventual dissolution of focal adhesions, so it is possible that the loss of PKA is coupled to one of those events. To better assess the kinetics of loss of PKA activity upon inhibition of contractility, we generated morphodynamic maps of protrusion/retraction velocities and PKA activity along the leading edge using QuimP11 edge tracking and sampling software (Bosgraaf and Van Haastert, 2010). As demonstrated previously (Tkachenko *et al.*, 2011), edge velocity and leading-edge PKA activity are spatiotemporally correlated in actively migrating cells (Figure 3D). Importantly, we also observed a rapid coincident decrease in edge dynamics and leading-edge PKA activity upon treatment with blebbistatin (Figure 3D).

While the observations in Figure 2 suggest that there is no spatial correlation between membrane-associated PKA signaling events and focal adhesion dynamics, focal adhesions are important centers of signal transduction and their dissolution upon inhibition of

contractility would be expected to disrupt that signaling. Specifically, if PKA activity were dependent on signaling from intact focal adhesions, we would predict that disassembly of focal adhesions would precede loss of PKA activity. Thus, we assessed the kinetics of inhibition of PKA activity relative to focal adhesion disassembly by measuring the rate of blebbistatin-induced loss of fluorescent signal intensity of two focal adhesion markers: zyxin, a mechanosensitive protein that leaves focal adhesion rapidly upon loss of contractility, and paxillin, which leaves "relaxed" focal adhesions much more slowly and with apparent zero-order kinetics (Zaidel-Bar *et al.*, 2003; Wolfenson *et al.*, 2011; Lavelin *et al.*, 2013). As expected, paxillin intensity within focal adhesions decreased slowly but steadily after blebbistatin treatment (Figure 3E), with an apparent half-life of 52.69 ± 3.35 min, while zyxin intensity decreased rapidly and exponentially, with a half-life of 7.63 ± 0.66 min (Figure 3E; Supplemental Movie S7), consistent with prior observations of the higher dependence of zyxin on mechanical forces for residence within focal adhesions (Lele *et al.*, 2006; Hirata *et al.*, 2008; Pasapera *et al.*, 2010; Wolfenson *et al.*, 2011; Lavelin *et al.*, 2013). Interestingly, PKA activity decreased even more rapidly after blebbistatin treatment than focal zyxin intensity (Figure 3E), with a half-life of ~50 s (0.83 ± 0.09 min). These observations are consistent with our observation of the lack of spatiotemporal correlation between focal adhesion dynamics and peripheral PKA signaling events and suggest a closer relative coupling of PKA to the contractile state of the cell. With this in mind, we then determined the kinetics of loss of cellular traction force after blebbistatin treatment using traction force microscopy on cells adhering to fibronectin-coated polyacrylamide hydrogels functionalized with fluorescent nanospheres (McKenzie *et al.*, 2018). As expected, cellular traction force decreased very rapidly after addition of blebbistatin, with a $t_{½}$ of 0.37 ± 0.05 min (Figure 3E and Supplemental Movie S8). While this $t_{½}$ value is likely to be erroneously high, given that the rate of image acquisition for these experiments (1 frame/min) results in an image interval that far exceeds the apparent $t_{½}$, it is consistent with published reports (Pasapera *et al.*, 2010; Wolfenson *et al.*, 2011; Lavelin *et al.*, 2013). More importantly, this decrease was far more rapid than the loss of paxillin or even zyxin from focal adhesions but only slightly more rapid than loss of PKA activity. Collectively, these data demonstrate that, during cell migration, regulation of PKA activity within the leading edge is kinetically coupled to and dependent on actomyosin contractility.

Spatial distribution of cellular traction forces and protein kinase activity during cell migration

If leading-edge PKA were regulated by actomyosin contractility, then one might expect PKA activity and cellular contractile forces to be coincident in migrating cells. To investigate this correlation directly, SKOV-3 cells expressing pmAKAR3 and migrating on nanosphere-functionalized hydrogels were analyzed by simultaneous FRET and traction force microscopy (TFM) in the absence and presence of blebbistatin (Figure 4). In the absence of blebbistatin, migrating cells exhibited high traction forces at sites of protrusion that overlapped with areas of high PKA activity (Figure 4A), and linescan analysis through cellular leading edges confirmed that the radial increase in PKA activity from cell center to periphery overlapped with peripherally increasing traction forces (Figure 4B). Of note, traction forces were significantly lower in spreading cells than in migrating cells (Supplemental Figure S7), consistent with the aforementioned lack of peripheral PKA activity in spreading cells (Figure 1). Importantly, both cellular traction forces and PKA activity decreased dramatically upon treatment with blebbistatin (Figure 4A), and the residual pockets of contractility were no longer spatially correlated with residual PKA activity (Figure 4C).

To formally quantify the extent to which PKA activity and traction forces overlap in migrating cells, TFM and FRET images were subjected to colocalization and intensity correlation analysis using intensity correlation quotients (ICQ). ICQ provide a single value indicating the covariance of two signals that can be used for statistical comparison (Li *et al.*, 2004; Jaskolski *et al.*, 2005). Mean ICQ values from –0.05 to +0.05 indicate random distribution of the two signals; values less than –0.05 indicate mutual exclusion; values between +0.05 and +0.1 indicate moderate covariance; and values >0.1 indicate strong covariance. Under control conditions, the mean ICQ for traction forces and PKA activity was 0.226 ± 0.022 and was significantly reduced to 0.032 ± 0.021 when the cells were treated with blebbistatin (mean ± SEM, Figure 4D). These data demonstrate that PKA activity and traction forces are spatially coincident in migrating cells. Coupled with the earlier observation that inhibition of actomyosin contractility significantly inhibits leading edge PKA activity, these observations strongly suggest that PKA activity is locally regulated by a contractility-dependent mechanotransduction pathway during cell migration.

Protein kinase is locally activated by acute mechanical stretch in an actomyosin-dependent manner

Given the demonstrated requirement of cellular tension for localized activation of PKA during migration, we wondered whether PKA might be locally activated by acute increases in cellular tension. Recently, it was shown that cellular mechanosensing is mediated not only by substrate rigidity but also by substrate deformation strain energy (Panzetta *et al.*, 2019). Thus, to test acute mechanical activation of PKA, cells expressing pmAKAR3 were plated onto fibronectin-coated hydrogels, and the hydrogel under individual cells was stretched (perpendicular to the axis of cell migration) with a microneedle (Supplemental Figure S5; Figure 5A; Svec *et al.*, 2019). This directional stretch produces a linear, inhomogeneous strain field (Supplemental Figure S8, A and B) between the cell and the probe. If one simplifies the elastic hydrogel to a series of equivalent springs, Hooke's Law ($F_P = k \times \Delta x$) dictates that a pulling force (F_P) applied to a spring results in a displacement (Δx) that is proportional to the spring's stiffness (k). Thus, the magnitude of the restoring force (i.e., the force required to restore the stretched spring to its original length) is proportional to how far the spring is stretched from its original length; that is, $F_R = -k \times \Delta x$. Because, in a locally stretched gel, the displacement increases with the proximity to the pulled microprobe (e.g., $\Delta x1 < \Delta x2 < \Delta x3$; Supplemental Figure S5, A and B), so then does the restoring force ($(F_{R1} = \bullet k \times \Delta x_1) < (F_{R2} = -k \times \Delta x_2) < (F_{R3} = -k \times \Delta x_3)$; Supplemental Figure 8C). At the cellular level, this increased force or countertension is perceived as a stiffer substrate. Specifically, as a cell probes this gradient (e.g., from *a* to *b* in Supplemental Figure S8A), either a "constant" cell-generated contractile force would produce less and less gel movement, or the cell would have to exert higher force in order to move the gel the same distance. In other words, because the restoring force increases in the direction of the pull, the *apparent* rigidity—as perceived by the cell—increases. The reader is referred to an elegant description of this in the original report of durotaxis (Lo *et al.*, 2000).

Application of directional stretch revealed a rapid (i.e., within 20 s), robust, and localized increase in PKA activity in the direction of stretch in both pmAKAR3-expressing cells (Figure 5, B–D; Supplemental Movie S9) and LynAKAR4-expressing cells (Supplemental Figure 3D), but not in cells expressing the phosphoresistant

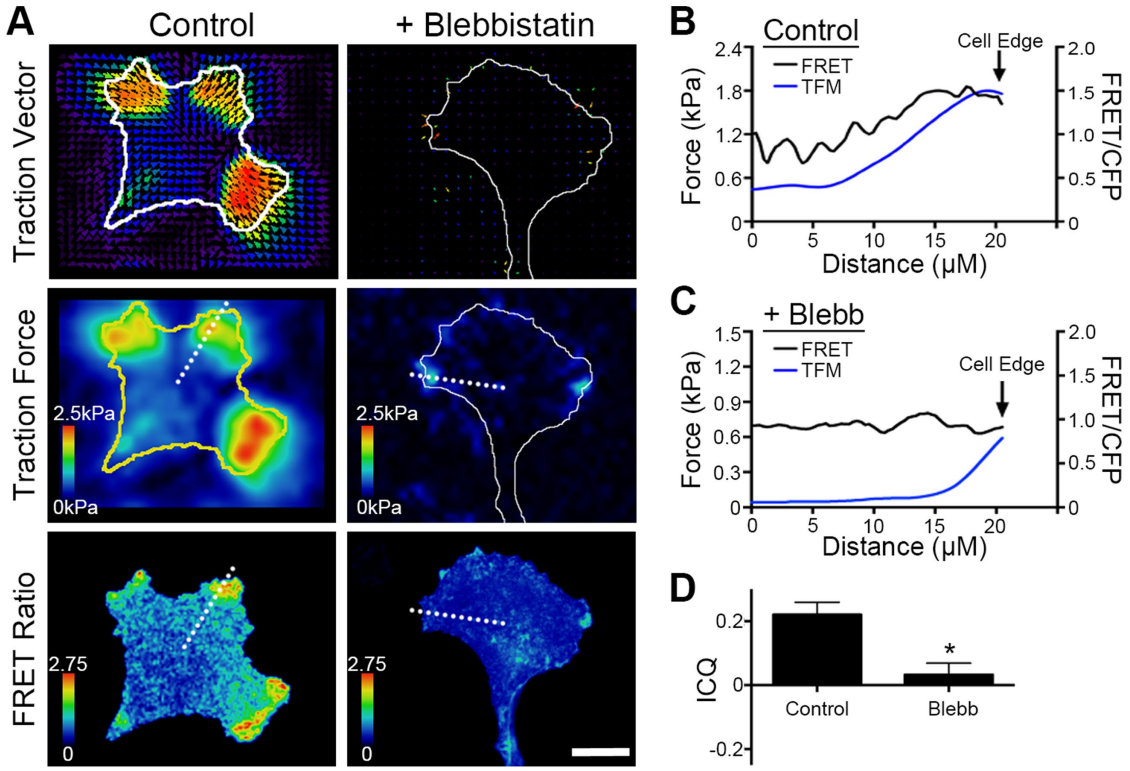

FIGURE 4: PKA activity and cellular traction forces are spatiotemporally correlated. (A) Cells expressing pmAKAR3 were plated on fibronectin-coated polyacrylamide hydrogels surface-conjugated with fluorescent 0.2 μm nanospheres and imaged by FRET microscopy and traction force microscopy after 20 min treatment with DMSO (Control) or 25 μM blebbistatin. The top panels show bead displacement/traction vector maps and the middle panels show traction force maps (with cell outlines plotted for reference) while the bottom panels show time-matched FRET/CFP images (bar = 10 μm). (B, C) Linescan analyses (dashed white lines in panel A) of both traction forces and FRET intensity from the cell centroid to the cell periphery for cells either control (B) or blebbistatin-treated (C) cells. (D) Pixel-by-pixel image correlation analysis was performed using intensity correlation analysis software (see *Materials and Methods*) to generate an intensity correlation quotient (ICQ). ICQs between traction force maps and PKA activity maps are summarized as mean ± SEM ($n = 7$ cells for each condition; $^*p < 0.001$).

pmAKAR3^{TA} biosensor (Supplemental Figure S9). Indeed, acute stretch appeared to "reorient" leading-edge PKA activity, as the increased activity seen proximal to stretch at the leading edge was often accompanied by decreased activity in other areas of the leading edge (Figure 5, C–E; Supplemental Movie S9). This activation was completely inhibited in cells coexpressing mCherry fused to the PKA-inhibitor protein (mCh-PKI; McKenzie *et al.*, 2011; Figure 5F), confirming the PKA specificity of the response. Importantly, acute mechanical activation of PKA was also completely inhibited in cells treated with blebbistatin before stretch (Figure 5F). These results show that acute mechanical stimulation can activate PKA in a manner that requires actomyosin contractility.

Protein kinase activity is required for durotaxis in SKOV-3 cells

Previously, we have shown that efficient migration in SKOV-3 cells is dependent upon PKA activity (McKenzie *et al.*, 2011). More recently, we showed that the migration of these cells is strongly influenced by the mechanical microenvironment and that these cells exhibit durotaxis, or mechanically guided migration toward regions of increased ECM rigidity and/or cell–matrix tension (McKenzie *et al.*, 2018). Given the current observations connecting cellular tension and stretch to activation of PKA, we investigated whether the durotactic migration of SKOV-3 might be similarly dependent on PKA activity. To this end, control cells or cells expressing mCh-PKI were cultured to migrate on fibronectin-coated hydrogels, subject to directional stretch as described above, and monitored for durotactic response (Svec *et al.*, 2019). While control cells exhibited robust durotaxis in response to acute directional stretch, inhibition of PKA activity dramatically decreased durotactic efficiency (Figure 6, A–C; Supplemental Movie S10). Taken together, these observations demonstrate that PKA activity is mechanically regulated during cell migration, is activated upon acute mechanical cell stretch, and is required for durotaxis.

DISCUSSION

The mechanosensitivity of cAMP/PKA signaling is well supported by the literature. For example, the cAMP cascade was the first mechanosensitive signaling cascade ever to be described (Rodan *et al.*, 1975). Also, the levels of cAMP and PKA activity have been shown to vary as a function of the mechanical tension of fibroblasts embedded in collagen gels (He and Grinnell, 1994). Furthermore, direct application of mechanical force through integrin-mediated adhesive contacts rapidly activates cAMP and PKA signaling and PKA-dependent transcription (Meyer *et al.*, 2000; Goldmann, 2002; Alenghat *et al.*, 2009). Finally, mechanical signals from fluid flow activate PKA in an ECM-specific manner (Funk *et al.*, 2010). While these and other studies firmly establish PKA as a mechanoresponsive target, it is important to note that they all assessed global rather than subcellular activation of cAMP/PKA and did not follow PKA dynamics in migrating cells.

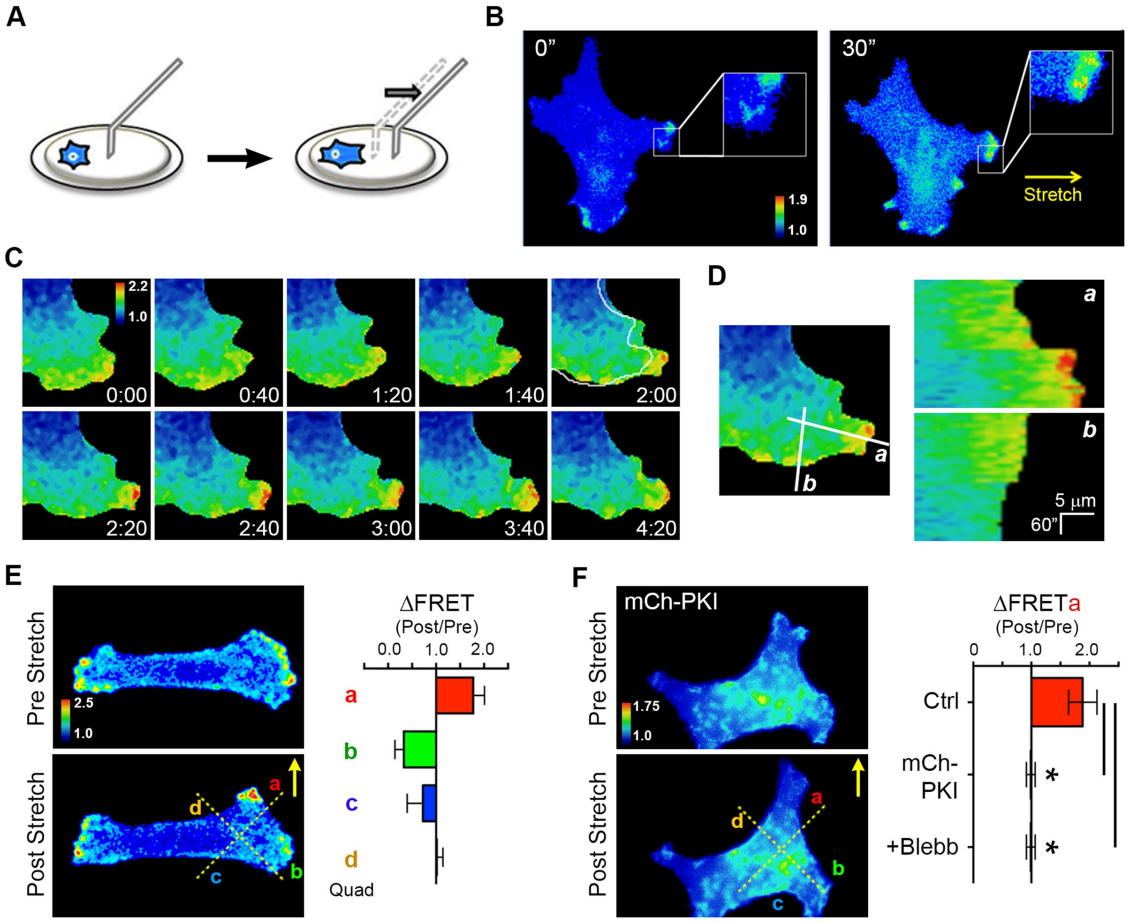

FIGURE 5: PKA is activated upon acute mechanical stretch and is required for SKOV-3 cell durotaxis. (A) Schematic of technique using a glass microneedle to impart acute directional stretch on individual cells by deformation of the underlying hydrogel (see text for details). (B) An SKOV-3 cell expressing pmAKAR3, plated on a hydrogel coated with fibronectin for 4 h and then imaged by FRET microscopy, before and 30 s after application of mechanical stretch by a microneedle in the direction indicated by the arrow. Warmer colors correspond to higher PKA activity as assessed by FRET ratio. (C) Time course of FRET ratio indicating PKA activity in an SKOV-3 cell expressing pmAKAR3 before and after application of mechanical stretch. Immediately before the 2:00 min mark, stretch was applied directly to the right of the panel. Deformation of the cell is highlighted by the outline of the cell before the stretch overlaid at 2:00 min. (D) Line scan analyses in the direction of (*a*) and orthogonal to the axis of stretch (*b*) show a unique increase in PKA activity along the axis of stretch after stimulation. (E) FRET ratio images were sectioned into quadrants *a* through *d*, depicted by dotted lines, for quantification of directional response. The change in PKA activity before and after stretch (ΔFRET) of SKOV-3 cells expressing pmAKAR3 was calculated in quadrants proximal (quadrant *a*), orthogonal (quadrants *b* and *d*), or contralateral (quadrant *c*) to the stretch (mean ± SEM; $n = 6$). (F) Change in PKA activity before and after stretch (ΔFRET) in quadrant *a* of SKOV-3 cells coexpressing pmAKAR3 and mCh-PKI (shown), coexpressing pmAKAR3 and mCherry, or SKOV-3 cells expressing only pmAKAR3 but pretreated with 25 µM blebbistatin (Blebb) for 10 min (mean ± SEM; $n = 9$ or 5 cells for control or mCh-PKI cells, respectively; $^*p < 0.005$ [Student's *t* test]).

Here, we demonstrate a link between cellular tension and regulation of subcellular PKA activity during cell migration. We show that leading- edge PKA activity correlates with the spatial distribution of cellular traction forces and that disruption of actomyosin contractility uncouples the spatial correlation between cellular forces and PKA activity. We establish that leading-edge PKA activity is regulated by cellular tension and show that locally applied mechanical forces elicit localized increases in PKA activity. Furthermore, we demonstrate that PKA activity is required for the durotactic response to directional mechanical cues, thereby expanding this enzyme's well-established role as a regulator of other modes of cell migration (Howe *et al.*, 2005; Lim *et al.*, 2008; Paulucci-Holthauzen *et al.*, 2009; McKenzie *et al.*, 2011; Tkachenko *et al.*, 2011). An intriguing recent report studying cells migrating from open to confined two-dimensional spaces showed that PKA activity was down-regulated during this transition in a manner dependent on Piezo1-mediated Ca^{2+} influx and, importantly, that leading-edge PKA activity appeared to increase upon treatment of cells with blebbistatin (Hung *et al.*, 2016). These latter observations are in direct contrast to the results reported here, which demonstrate a decrease in PKA activity upon treatment not only with blebbistatin, but also with other "upstream" inhibitors of actomyosin contractility (Y-27632, H-1152, fasudil/HA1077, and ML7; Figure 3). The reasons for this disparity are currently unknown but may include differences in cell lines and culture conditions. The prior study saw increased PKA activity after blebbistatin treatment (in both confined and unconfined cells) using CHO-K1 cells and a derivative line expressing the α4 integrin (CHO-α4WT), adhering to surfaces coated with 20 µg/ml

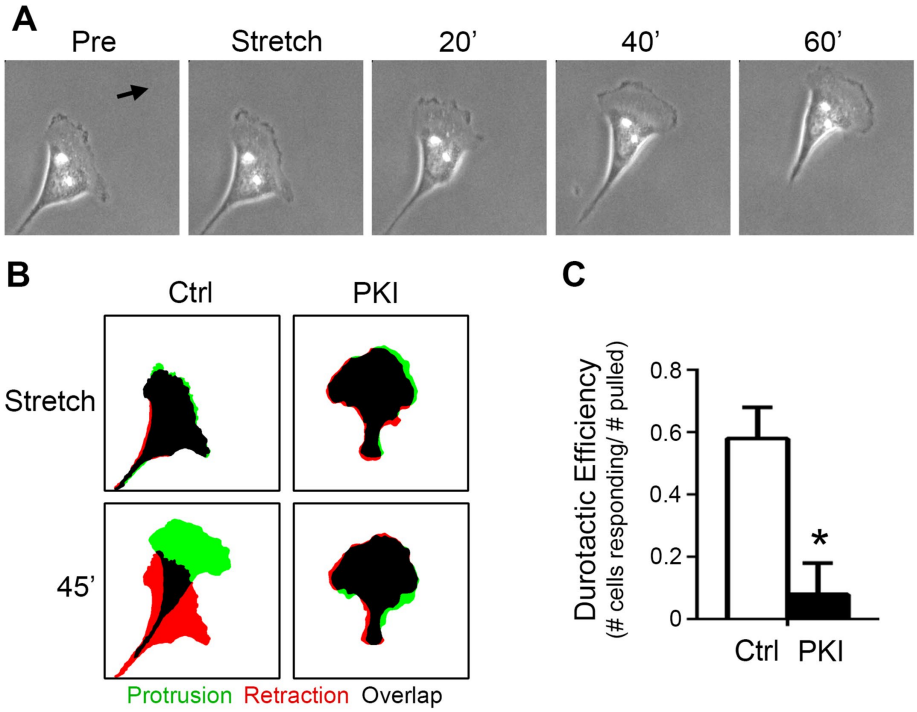

FIGURE 6: PKA is required for SKOV-3 cell durotaxis. (A) An SKOV-3 cell plated onto a 25-kPa fibronectin-coated hydrogel for 4 h was monitored by live-cell phase-contrast microscopy before and after durotactic stimulation (in the direction indicated by the arrow); images captured 1 min before (Pre) application of stretch, one minute after application (Stretch), and every 20 min thereafter are shown. (B) Control cells or cells expressing mCherry–PKI (PKI) were cultured and stimulated to invoke durotaxis as described for panel A. Protrusion/retraction analysis maps (PRAMs) were generated from manually thresholded and outlined phase-contrast images taken 1 min before and 1 min after stretch (Stretch) and 1 min and 45 min after stretch (45′) to identify regions of protrusion, retraction, and overlap (green, red, and black, respectively). (C) Durotactic efficiency (see *Materials and Methods* for details) was calculated for control and mCherry–PKI-expressing cells ($n = 8$ for each condition; $*p < 0.01$).

fibronectin. These are notable, yet modest differences compared with those in the current work, which uses SKOV-3 cells adhering to fibronectin at 10 µg/ml.

While it will be important to keep these differences in mind for future studies, it is perhaps more important to appreciate that, together, the two reports firmly establish PKA as a target for mechanical regulation during migration. Moreover, given the importance of mechanotransduction in regulating cell adhesion and motility (Schwartz and DeSimone, 2008; Roca-Cusachs *et al.*, 2013; Schiller and Fassler, 2013) and the long and growing list of adhesion-related and cytoskeletal targets for PKA (Howe and Juliano, 2000; Howe *et al.*, 2002, 2005; Howe, 2004, 2011; Lim *et al.*, 2007; Tkachenko *et al.*, 2011; Yeo *et al.*, 2011; Takahashi *et al.*, 2013; Ithychanda *et al.*, 2015; Nagy *et al.*, 2015; Robertson *et al.*, 2015; Chavez-Vargas *et al.*, 2016; Gau *et al.*, 2019; Tonucci *et al.*, 2019), the demonstration that PKA activity can be dynamically and locally regulated by cell tension provides an important new axis of regulation. Though the current work establishes the connection between leading-edge PKA activity and actomyosin contractility, the exact molecular mechanism coupling cellular tension to localized PKA activity remains to be elucidated. A plausible hypothesis is that canonical activators of the cAMP/PKA pathway (G-protein coupled receptors, adenylyl cyclases, or phosphodiesterases) are locally and mechanically regulated during cell migration. Importantly, GPCRs are well-established mediators of mechanotransduction (Storch *et al.*, 2012), and experiments imparting tension across fibronectin-coated magnetic beads have demonstrated that force application to integrins led to activation PKA in a Gαs-dependent manner (Meyer *et al.*, 2000; Alenghat *et al.*, 2009). Efforts to investigate the possible role of GPCR signaling in mechanically regulated PKA activity are currently under way.

Previous work has shown activation of leading-edge PKA activity to be integrin-mediated (O'Connor and Mercurio, 2001; Whittard and Akiyama, 2001; Howe *et al.*, 2002; Gui *et al.*, 2006; Lim *et al.*, 2007, 2008; Goldfinger *et al.*, 2008; Funk *et al.*, 2010). However, the current observations establish that this activity is both spatially and temporally distinct from sites of integrin-dependent focal adhesion assembly. It is important to reiterate that we cannot rule out a contribution of direct, integrin-mediated signaling events arising from focal complexes that are below the level of detection using the current methods. However, we contend that the circuitry for localized activation of PKA is spatially, temporally, and thus biochemically separate from mature focal adhesions. Moreover, we do not contend that focal adhesions are wholly unnecessary for regulating PKA during migration. As the nexus between the actin cytoskeleton and matrix-bound integrins, focal adhesions are principal mediators of mechanical signaling. However, the relative kinetics of PKA inactivation and focal adhesion disassembly suggests that PKA is regulated by a tension-dependent aspect/characteristic of intact focal adhesions (e.g., a mechanically regulated enzymatic activity or protein–protein interaction) rather than direct focal adhesion assembly or disassembly per se.

It is also important to restate here that the current study used the targeted biosensors pmAKAR3 and Lyn-AKAR4, which report only plasma membrane– and lipid raft–proximal PKA events, respectively. The machinery for generating, sensing, and transducing mechanical signals extends well beyond membranes—from the extracellular matrix, through transmembrane integrins and their associated juxta–membrane complexes, to deep inside the cell (Ingber, 1997; Bershadsky *et al.*, 2003; Janmey and McCulloch, 2007; Schwartz, 2010; Horton *et al.*, 2016). In addition, paradigm-shifting recent work has shown that PKA signaling can occur not necessarily through release of a diffusible catalytic subunit but through intact, anchored holoenzymes (Smith *et al.*, 2017), exchanging action at a distance for a far more localized, almost "solid-state" activity. This paradigm of highly localized PKA activity may be particularly important for mediating its effects on architectural and scaffolding structures (e.g., actin microfilaments, focal adhesions) associated with cell migration. Thus, given the physical span of mechanotransduction machinery and this recent appreciation of the limited radius in which anchored PKA signaling may take place, there very well may be other pools of highly localized PKA activity that are important for migration but are not readily detected by membrane-targeted biosensors. With the wide and growing variety of AKAPs (Diviani and Scott, 2001; Skroblin *et al.*, 2010;

Scott *et al.*, 2013) and the myriad known and potential substrates for PKA present in various cellular regions and structures involved in cell migration (discussed above), it would be of considerable interest (and complexity) to evaluate PKA activity using a series of biosensors targeted to distinct migration-associated domains or structures to identify structure-specific dynamics and substrates, and thus more fully dissect the contributions of PKA to cell motility.

MATERIALS AND METHODS

Reagents and cell culture

Human epithelial ovarian cancer (SKOV-3) cells were purchased from the American Type Culture Collection, authenticated at the UVM Advanced Genomic Technology Core, and maintained in a humidified incubator at 37°C containing 5% CO_2 in DMEM supplemented with 10% fetal bovine serum. All cell lines in the laboratory were checked for mycoplasma monthly by DAPI (4′,6-diamidino-2-phenylindole) staining and every 4–6 mo using a commercial kit (MycoAlert, Lonza). Cells were trypsinized and split 1:5 every 3–4 d to avoid reaching confluence. Cells were transfected using Fugene6 (Promega) according to the manufacturer's protocol. In brief, cells were plated into 35-mm dishes at 60–70% confluence the day before transfection so that they were 75–85% confluent at the time of transfection. Fugene6 and Opti-MEM were warmed to room temperature (RT) and 6 µl of Fugene6 was diluted into 100 µl of Opti-MEM, vortexed, and incubated for 5 min at RT. A total of 1.5 µg of plasmid DNA was added to the diluted Fugene6 at a 1:4 ratio (1.5 µg DNA/6 µl Fugene6), vortexed, and incubated for 15 min at RT. The transfection solution was then added dropwise to cells and images were acquired 48 h posttransfection.

Blebbistatin, fasudil, H-1152, and ML7 were purchased from Tocris. Acrylamide and N,N′-methylenebisacrylamide were purchased from National Diagnostics. Tetramethylethylenediamine (TEMED), ammonium persulfate (APS), and bovine serum albumin (BSA), along with other sundry chemicals, were purchased from Sigma (St. Louis, MO). Plasmids used in this work included PKA biosensor pmAKAR3 (Allen and Zhang, 2006) from Jin Zhang (Johns Hopkins University); pYFP-dSH2 from Benny Geiger (Weizmann Institute of Science); and pmCherry-FAK and pRFP-zyxin from Addgene (plasmids #35039 and 26720, respectively). The plasmid encoding mCherry–paxillin was made by substituting mCherry for EGFP in pEGFP-N1-paxillin (a gift from Chris Turner, SUNY, Upstate), while the PKA inhibitor peptide fused to mCherry (mCherry-PKI) was described previously (McKenzie *et al.*, 2011).

Fabrication of polyacrylamide hydrogels

Acrylamide hydrogels with a Young's elastic modulus of ~25 kPa were fabricated essentially as described previously (McKenzie *et al.*, 2018; Svec *et al.*, 2019). Briefly, cleaned 25 mm–diameter round glass coverslips were briefly flamed and incubated with 0.1 N NaOH for 15 min. After removal of excess NaOH, 25 µl (3-aminopropyl)-trimethoxysilane (APTMS) was smeared on the coverslips and incubated for 3 min at RT and the coverslips were washed 3 × 5 min in ddH_2O and dried by aspiration. Once dried, the coverslips were incubated with 500 µl 0.5% glutaraldehyde for 30 min. The glutaraldehyde was removed and a 25-µl drop of acrylamide solution (7.5:0.5% acrylamide:bis-acrylamide, activated with APS and TEMED) was sandwiched between the activated coverslip and a 22 mm–diameter coverslip passivated with RainX (ITW Global Brands, Houston, TX) and allowed to polymerize for 10 min. Once polymerized, the RainX-treated coverslip was removed and the hydrogel was washed three times (5 min each) in PBS. The gel surface was derivatized with the heterobifunctional cross-linker sulfo-SANPAH as previously described (Tse and Engler, 2010; McKenzie *et al.*, 2018; Svec *et al.*, 2019). For routine studies, activated gels were functionalized with 20 µg/ml fibronectin at 37°C for 45 min. For traction force microscopy studies, 0.2 µm red fluorescent carboxy-modified latex microspheres (Invitrogen, F8810) were conjugated to the gel surface by incubating a sonicated suspension of the beads (1:200 in 50 mM HEPES, pH 8.5) on the gels for 30 min. The gels were rinsed three times with 50 mM HEPES (pH 8.5) to remove all nonattached beads and then incubated with 20 µg/ml fibronectin (diluted in 50 mM HEPES, pH 8.5) at 37°C for 45 min. The gels were postfixed with 0.5% glutaraldehyde for 1 h at RT and quenched in $NaBH_4$ before cells were plated in complete media. Coated gels were washed 3 × 5 min in PBS and either used immediately or stored at 4°C for up to 1 wk. In some experiments, hydrogels were cast in a similar manner directly onto the surface of glass-bottomed imaging dishes (Delta T; Bioptechs) instead of 25-mm coverslips.

Live cell imaging

Cells transfected with plasmids encoding pmAKAR3 were cultured overnight in serum-free DMEM + 40 ng/ml epidermal growth factor (EGF), trypsinized, soybean trypsin inhibitor added, pelleted, and resuspended in DMEM 1% BSA + 25 or 40 ng/ml EGF. These cells were plated on fibronectin-coated coverslips and incubated for ~4 h before imaging at low density to induce migration. Cells plated on hydrogels for durotaxis were incubated overnight in complete media then rinsed twice in modified Ringer's buffer without phosphate (10 mM HEPES; 10 mM glucose; 155 mM NaCl; 5 mM KCl; 2 mM $CaCl_2$; 1 mM $MgCl_2$). All cells were refed modified Ringer's buffer supplemented with 25 or 40 ng/ml EGF for imaging. Coverslips were mounted in a chamber (Attofluor; ThermoFisher) before imaging. Culture temperature was maintained at 35–37°C with hot air (ASI 400 Air Stream; Nevtek). Cultures of hydrogels cast in imaging dishes were mounted, warmed, and imaged in a suitable temperature controller (Delta T4; Bioptechs).

Durotaxis assay

Cells were seeded on fibronectin-coated gels and mounted and maintained on the microscope as above. Cells were manipulated with a glass microneedle as described previously (Wang *et al.*, 2001; McKenzie *et al.*, 2018; Svec *et al.*, 2019). Briefly, micropipettes were fashioned from borosilicate glass capillaries (1B150-4 or TW150-4; World Precision Instruments) on a two-stage pipette puller (Pul-2; World Precision Instruments). A Narishige MF-900 microforge was used to form the micropipette tip into a hooked probe with a rounded end to engage the polyacrylamide hydrogels without tearing. The probe was mounted on a micromanipulator (Leitz or Narishige) and lowered onto the gel surface ~20 µm away from a cell and pulled 20 µm in a direction orthogonal to the cell's long axis. Quantification of response to stretch was calculated using custom ImageJ Protrusion-Retraction Analysis Mapping (PRAM) macros designed to calculate the percentage of cell area protruding, retracting, and overlapping between any two given frames of time-lapse images (Deming *et al.*, 2015). A positive durotactic response was defined as a >50% increase in the protrusion index (protrusion area/[protrusion area + overlap area]) in the direction of stretch over 45 min, and durotactic efficiency was defined as the number of cells showing a durotactic response divided by the number of cells pulled.

Förster resonance energy transfer imaging and analysis

The FRET-based PKA activity biosensor pmAKAR3, consisting of a sensor cassette (i.e., a PKA-specific substrate domain and a flanking

phosphoamino acid–binding FHA1 (forkhead-associated domain-1) located between ECFP and an EYFP variant (circularly permuted Venus cpV-E172; Allen and Zhang, 2006), and a C-terminal CAAX box (derived from K-Ras) for targeting to the plasma membrane, was imaged in SKOV-3 cells as previously described (McKenzie *et al.*, 2011). Briefly, 48 h after transfection, cells were rinsed twice and maintained in a HEPES-buffered saline solution containing (in mM) 134 NaCl, 5.4 KCl, 1.0 $MgSO_4$, 1.8 $CaCl_2$, 20 HEPES, and 5 D-glucose (pH 7.4) without serum, unless otherwise specified. Cells were imaged on a Nikon Eclipse TE-2000E inverted microscope with a 60×/1.4NA Plan Apo oil-immersion objective lens using the appropriate fluorophore-specific filters (Chroma Technology, Rockingham, VT) and an Andor Clara charged coupled device camera (Andor Technologies, South Windsor, CT) controlled by Elements (Nikon) software. CFP, YFP, and FRET images were acquired with (400–700)-ms exposures and 2 × 2 binning for each acquisition at 60-s intervals, unless otherwise noted in the figure legends. Images in each channel were subjected to background subtraction, and FRET ratios were calculated using either the Biosensors FRET ImageJ plug-in (Hodgson *et al.*, 2010) or a slightly modified mathematical protocol as described elsewhere (Broussard *et al.*, 2013). Pseudocolor images were generated using a custom-written ImageJ look-up table.

Cell spreading and migration assays

To monitor cell spreading, cells were prepared and cultured as previously described (Howe *et al.*, 2002). Briefly, cells were serum-starved overnight, trypsinized, quenched with 1 mg/ml soybean trypsin inhibitor, washed via centrifugation (50 × *g* for 5 min), resuspended in DMEM 1% BSA, and rocked for 1 h before being plated on fibronectin-coated (10 µg/ml) glass-bottomed imaging dishes. The cells were allowed to settle to the bottom of the dish for 10 min at 4°C before imaging as described below. Similar conditions were used to monitor migrating cells, with the exception that the cells were allowed to adhere, spread, and begin migrating for 4 h at 37°C before imaging. Cells were imaged in Ringer's buffer.

Correlating edge velocity and protein kinase activity

Corrected FRET ratio time-lapse movies were fed to the Quantitative Imaging of Membrane Proteins (QuimP11) package (http://go.warwick.ac.uk/bretschneider/quimp) software, which analyzed edge dynamics and calculated edge velocity. Additionally, the software generated two-dimensional morphodynamic plots of edge velocities along the cell edge over time and computed autocorrelation coefficients of edge dynamics. Once edge dynamics was analyzed, the corrected FRET ratio images were analyzed by QuimP11 to sample the FRET ratios within 10 µm of the cell edge. The software generated two-dimensional heat maps of PKA activity along the cell edge over time and calculated cross-correlation coefficients at different time lags to determine when peak PKA activity events were occurring in relation to peak protrusion events. The ImageJ plug-in, QuimP11, was also used to display time-coded depth stacks to depict cell movement over time in a single image.

Focal adhesion analysis

Cells were transfected with plasmids encoding focal adhesion markers (mCherry–paxillin, mCherry–FAK, or RFP–zyxin) and either pmAKAR3 or dSH2-YFP to visualize focal adhesions and PKA activity or tyrosine phosphorylation. Images were acquired at 60-s intervals. Focal-adhesion pixel intensities and lifetimes were calculated by manually thresholding adhesions and measuring pixel intensities, adhesion assembly and disassembly rates, and lifetimes of individual adhesions in time-lapse movies. To quantify the spatiotemporal correlation between focal adhesion dynamics and PKA activity, leading-edge focal adhesions were tracked over time and an interrogation region of interest (ROI) that was 50% larger than the area of the adhesion was used to track pmAKAR3 FRET ratios in the same cellular regions. Pearson's correlation coefficients were generated using the Intensity Correlation Analysis ImageJ plug-in, and average values are represented as mean ± SEM. LynAKAR4 FRET and mCherry–Paxillin signals were analyzed by overlaying the thresholded peak signals (≥85% of maximum).

Traction force microscopy

TFM was performed essentially as described previously (McKenzie *et al.*, 2018). Briefly, cells were plated on polyacrylamide gels that were surface-conjugated with 0.2-µm red fluorescent latex microspheres as described above. Cells were adhered to the hydrogels overnight in complete media and were washed twice and maintained in HEPES-buffered saline as described above. Coverslips were mounted in imaging chambers as above and fluorescent bead images were captured though a 20× Plan Apo objective on a Nikon Eclipse TE-2000E inverted microscope as described above. Bead images were acquired before and after cells were cleared by the addition of trypsin/EDTA (0.5%). Cell outlines were generated using either the YFP image from cells expressing pmAKAR3 or a transmitted light image in cases where cells were not transfected. Bead images were registered to correct for any stage drift; then the movement of individual microspheres between image pairs was calculated using particle image velocimetry (PIV) and the Young's elastic modulus of the polyacrylamide hydrogels (25 kPa) was used to calculate traction forces using Fourier transform traction cytometry (FTTC; Marinkovic *et al.*, 2012; Tseng *et al.*, 2012). The mean traction force within the cell was used to generate the average cellular traction and the mean of the maximum traction forces was used to generate the average maximum traction force generation.

Traction force microscopy/Förster resonance energy transfer correlation analysis

To correlate cellular traction forces and PKA activity, both readings were captured simultaneously and analyzed independently. Once heat maps of both PKA activity and traction forces were generated, standard image correlation analysis was performed. This analysis was made possible because the two signals are rendered as 8-bit gray-scale images and higher pixel intensity corresponds with either higher PKA activity or higher traction forces. Lookup tables are assigned to the images after analysis for ease of interpreting biosensor and TFM data. Mander's correlation coefficients and intensity correlation quotients were generated using the Intensity Correlation Analysis ImageJ plug-in, and average values are represented as mean ± SEM. Intensity correlation quotient (ICQ) analysis has been described in detail elsewhere. In brief, ICQ reflects the ratio of the number of positive (*Ai-al*)(*Bi-b*) values to the total number of pixels in the region of interest, where *a* and *b* are the means of each signal intensity's values *Ai* and *Bi*. ICQ values from -0.05 to +0.05 indicate random (noncovariant) signals, 0.05–0.1 indicate weak covariance, and >0.1 indicates strong covariance.

ACKNOWLEDGMENTS

We thank Benny Geiger (Weitzmann Institute), Jin Zhang (Johns Hopkins University), and Chris Turner (SUNY–Upstate) for generously providing plasmids. This work was supported by National Institute of General Medical Sciences (NIGMS) Grants R01GM097495

and R01GM117490 (to A.K.H.) and R01GM097495-S1 (A.J.McK.) and a University of Vermont College of Medicine Pilot Project Award (A.K.H.).

REFERENCES

Alenghat FJ, Tytell JD, Thodeti CK, Derrien A, Ingber DE (2009). Mechanical control of cAMP signaling through integrins is mediated by the heterotrimeric Galphas protein. J Cell Biochem 106, 529–538.

Allen MD, Zhang J (2006). Subcellular dynamics of protein kinase A activity visualized by FRET-based reporters. Biochem Biophys Res Commun 348, 716–721.

Amano M, Ito M, Kimura K, Fukata Y, Chihara K, Nakano T, Matsuura Y, Kaibuchi K (1996). Phosphorylation and activation of myosin by Rho-associated kinase (Rho-kinase). J Biol Chem 271, 20246–20249.

Aratyn-Schaus Y, Gardel ML (2010). Transient frictional slip between integrin and the ECM in focal adhesions under myosin II tension. Curr Biol 20, 1145–1153.

Balaban NQ, Schwarz US, Riveline D, Goichberg P, Tzur G, Sabanay I, Mahalu D, Safran S, Bershadsky A, Addadi L, Geiger B (2001). Force and focal adhesion assembly: a close relationship studied using elastic micropatterned substrates. Nat Cell Biol 3, 466–472.

Beningo KA, Dembo M, Kaverina I, Small JV, Wang YL (2001). Nascent focal adhesions are responsible for the generation of strong propulsive forces in migrating fibroblasts. J Cell Biol 153, 881–888.

Bereiter-Hahn J, Luers H (1998). Subcellular tension fields and mechanical resistance of the lamella front related to the direction of locomotion. Cell Biochem Biophys 29, 243–262.

Bershadsky AD, Balaban NQ, Geiger B (2003). Adhesion-dependent cell mechanosensitivity. Annu Rev Cell Dev Biol 19, 677–695.

Bosgraaf L, Van Haastert PJ (2010). Quimp3, an automated pseudopod-tracking algorithm. Cell Adh Migr 4, 46–55.

Broussard JA, Rappaz B, Webb DJ, Brown CM (2013). Fluorescence resonance energy transfer microscopy as demonstrated by measuring the activation of the serine/threonine kinase Akt. Nat Protoc 8, 265–281.

Burnette DT, Ji L, Schaefer AW, Medeiros NA, Danuser G, Forscher P (2008). Myosin II activity facilitates microtubule bundling in the neuronal growth cone neck. Dev Cell 15, 163–169.

Chavez-Vargas L, Adame-Garcia SR, Cervantes-Villagrana RD, Castillo-Kauil A, Bruystens JG, Fukuhara S, Taylor SS, Mochizuki N, Reyes-Cruz G, Vazquez-Prado J (2016). Protein kinase A (PKA) type I interacts with P-Rex1, a Rac guanine nucleotide exchange factor: effect on pka localization and P-Rex1 signaling. J Biol Chem 291, 6182–6199.

Choquet D, Felsenfeld DP, Sheetz MP (1997). Extracellular matrix rigidity causes strengthening of integrin-cytoskeleton linkages. Cell 88, 39–48.

Chrzanowska-Wodnicka M, Burridge K (1996). Rho-stimulated contractility drives the formation of stress fibers and focal adhesions. J Cell Biol 133, 1403–1415.

Del Pozo MA (2004). Integrin signaling and lipid rafts. Cell Cycle 3, 725–728.

del Pozo MA, Alderson NB, Kiosses WB, Chiang HH, Anderson RG, Schwartz MA (2004). Integrins regulate Rac targeting by internalization of membrane domains. Science 303, 839–842.

del Pozo MA, Balasubramanian N, Alderson NB, Kiosses WB, Grande-Garcia A, Anderson RG, Schwartz MA (2005). Phospho-caveolin-1 mediates integrin-regulated membrane domain internalization. Nat Cell Biol 7, 901–908.

Delint-Ramirez I, Willoughby D, Hammond GR, Ayling LJ, Cooper DM (2011). Palmitoylation targets AKAP79 protein to lipid rafts and promotes its regulation of calcium-sensitive adenylyl cyclase type 8. J Biol Chem 286, 32962–32975.

Dembo M, Wang YL (1999). Stresses at the cell-to-substrate interface during locomotion of fibroblasts. Biophys J 76, 2307–2316.

Deming PB, Campbell SL, Stone JB, Rivard RL, Mercier AL, Howe AK (2015). Anchoring of protein kinase A by ERM (ezrin-radixin-moesin) proteins is required for proper netrin signaling through DCC (deleted in colorectal cancer). J Biol Chem 290, 5783–5796.

Depry C, Allen MD, Zhang J (2011). Visualization of PKA activity in plasma membrane microdomains. Mol Biosyst 7, 52–58.

Diviani D, Scott JD (2001). AKAP signaling complexes at the cytoskeleton. J Cell Sci 114, 1431–1437.

Fabbri M, Di Meglio S, Gagliani MC, Consonni E, Molteni R, Bender JR, Tacchetti C, Pardi R (2005). Dynamic partitioning into lipid rafts controls the endo-exocytic cycle of the alphaL/beta2 integrin, LFA-1, during leukocyte chemotaxis. Mol Biol Cell 16, 5793–5803.

Funk SD, Yurdagul A Jr, Green JM, Jhaveri KA, Schwartz MA, Orr AW (2010). Matrix-specific protein kinase A signaling regulates p21-activated kinase activation by flow in endothelial cells. Circ Res 106, 1394–1403.

Gagnoux-Palacios L, Dans M, van't Hof W, Mariotti A, Pepe A, Meneguzzi G, Resh MD, Giancotti FG (2003). Compartmentalization of integrin alpha6beta4 signaling in lipid rafts. J Cell Biol 162, 1189–1196.

Gau D, Veon W, Shroff SG, Roy P (2019). The VASP-profilin1 (Pfn1) interaction is critical for efficient cell migration and is regulated by cell-substrate adhesion in a PKA-dependent manner. J Biol Chem 294, 6972–6985.

Gaus K, Le Lay S, Balasubramanian N, Schwartz MA (2006). Integrin-mediated adhesion regulates membrane order. J Cell Biol 174, 725–734.

Giannone G, Dubin-Thaler BJ, Rossier O, Cai Y, Chaga O, Jiang G, Beaver W, Dobereiner HG, Freund Y, Borisy G, Sheetz MP (2007). Lamellipodial actin mechanically links myosin activity with adhesion-site formation. Cell 128, 561–575.

Goldfinger LE, Tzima E, Stockton R, Kiosses WB, Kinbara K, Tkachenko E, Gutierrez E, Groisman A, Nguyen P, Chien S, Ginsberg MH (2008). Localized alpha4 integrin phosphorylation directs shear stress-induced endothelial cell alignment. Circ Res 103, 177–185.

Goldmann WH (2002). The coupling of vinculin to the cytoskeleton is not essential for mechano-chemical signaling in F9 cells. Cell Biol Int 26, 279–286.

Golub T, Caroni P (2005). PI(4,5)P2-dependent microdomain assemblies capture microtubules to promote and control leading edge motility. J Cell Biol 169, 151–165.

Gui P, Wu X, Ling S, Stotz SC, Winkfein RJ, Wilson E, Davis GE, Braun AP, Zamponi GW, Davis MJ (2006). Integrin receptor activation triggers converging regulation of Cav1.2 calcium channels by c-Src and protein kinase A pathways. J Biol Chem 281, 14015–14025.

He Y, Grinnell F (1994). Stress relaxation of fibroblasts activates a cyclic AMP signaling pathway. J Cell Biol 126, 457–464.

Head BP, Patel HH, Insel PA (2014). Interaction of membrane/lipid rafts with the cytoskeleton: impact on signaling and function: membrane/lipid rafts, mediators of cytoskeletal arrangement and cell signaling. Biochim Biophys Acta 1838, 532–545.

Hirata H, Tatsumi H, Sokabe M (2008). Mechanical forces facilitate actin polymerization at focal adhesions in a zyxin-dependent manner. J Cell Sci 121, 2795–2804.

Hodgson L, Shen F, Hahn K (2010). Biosensors for characterizing the dynamics of rho family GTPases in living cells. Curr Protoc Cell Biol Chapter 14, Unit 14 11 11–26.

Horton ER, Astudillo P, Humphries MJ, Humphries JD (2016). Mechanosensitivity of integrin adhesion complexes: role of the consensus adhesome. Exp Cell Res 343, 7–13.

Hotulainen P, Lappalainen P (2006). Stress fibers are generated by two distinct actin assembly mechanisms in motile cells. J Cell Biol 173, 383–394.

Howe AK (2004). Regulation of actin-based cell migration by cAMP/PKA. Biochim Biophys Acta 1692, 159–174.

Howe AK (2011). Cross-talk between calcium and protein kinase A in the regulation of cell migration. Curr Opin Cell Biol 23, 554–561.

Howe AK, Baldor LC, Hogan BP (2005). Spatial regulation of the cAMP-dependent protein kinase during chemotactic cell migration. Proc Natl Acad Sci USA 102, 14320–14325.

Howe AK, Hogan BP, Juliano RL (2002). Regulation of vasodilator-stimulated phosphoprotein phosphorylation and interaction with Abl by protein kinase A and cell adhesion. J Biol Chem 277, 38121–38126.

Howe AK, Juliano RL (2000). Regulation of anchorage-dependent signal transduction by protein kinase A and p21-activated kinase. Nat Cell Biol 2, 593–600.

Humphries JD, Chastney MR, Askari JA, Humphries MJ (2019). Signal transduction via integrin adhesion complexes. Curr Opin Cell Biol 56, 14–21.

Hung WC, Yang JR, Yankaskas CL, Wong BS, Wu PH, Pardo-Pastor C, Serra SA, Chiang MJ, Gu Z, Wirtz D, *et al*. (2016). Confinement sensing and signal optimization via Piezo1/PKA and myosin II pathways. Cell Rep 15, 1430–1441.

Ingber DE (1997). Integrins, tensegrity, and mechanotransduction. Gravit Space Biol Bull 10, 49–55.

Ithychanda SS, Fang X, Mohan ML, Zhu L, Tirupula KC, Naga Prasad SV, Wang YX, Karnik SS, Qin J (2015). A mechanism of global shape-dependent recognition and phosphorylation of filamin by protein kinase A. J Biol Chem 290, 8527–8538.

Janmey PA, McCulloch CA (2007). Cell mechanics: integrating cell responses to mechanical stimuli. Annu Rev Biomed Eng 9, 1–34.

Jaskolski F, Mulle C, Manzoni OJ (2005). An automated method to quantify and visualize colocalized fluorescent signals. J Neurosci Methods 146, 42–49.
Kirchner J, Kam Z, Tzur G, Bershadsky AD, Geiger B (2003). Live-cell monitoring of tyrosine phosphorylation in focal adhesions following microtubule disruption. J Cell Sci 116, 975–986.
Kolega J (2004). Phototoxicity and photoinactivation of blebbistatin in UV and visible light. Biochem Biophys Res Commun 320, 1020–1025.
Lavelin I, Wolfenson H, Patla I, Henis YI, Medalia O, Volberg T, Livne A, Kam Z, Geiger B (2013). Differential effect of actomyosin relaxation on the dynamic properties of focal adhesion proteins. PLoS One 8, e73549.
Leitinger B, Hogg N (2002). The involvement of lipid rafts in the regulation of integrin function. J Cell Sci 115, 963–972.
Lele TP, Pendse J, Kumar S, Salanga M, Karavitis J, Ingber DE (2006). Mechanical forces alter zyxin unbinding kinetics within focal adhesions of living cells. J Cell Physiol 207, 187–194.
Levayer R, Lecuit T (2012). Biomechanical regulation of contractility: spatial control and dynamics. Trends Cell Biol 22, 61–81.
Li Q, Lau A, Morris TJ, Guo L, Fordyce CB, Stanley EF (2004). A syntaxin 1, Galpha(o), and N-type calcium channel complex at a presynaptic nerve terminal: analysis by quantitative immunocolocalization. J Neurosci 24, 4070–4081.
Lim CJ, Han J, Yousefi N, Ma Y, Amieux PS, McKnight GS, Taylor SS, Ginsberg MH (2007). Alpha4 integrins are type I cAMP-dependent protein kinase-anchoring proteins. Nat Cell Biol 9, 415–421.
Lim CJ, Kain KH, Tkachenko E, Goldfinger LE, Gutierrez E, Allen MD, Groisman A, Zhang J, Ginsberg MH (2008). Integrin-mediated protein kinase A activation at the leading edge of migrating cells. Mol Biol Cell 19, 4930–4941.
Lintz M, Munoz A, Reinhart-King CA (2017). The mechanics of single cell and collective migration of tumor cells. J Biomech Eng 139, 0210051.
Lo CM, Wang HB, Dembo M, Wang YL (2000). Cell movement is guided by the rigidity of the substrate. Biophys J 79, 144–152.
Marinkovic A, Mih JD, Park JA, Liu F, Tschumperlin DJ (2012). Improved throughput traction microscopy reveals pivotal role for matrix stiffness in fibroblast contractility and TGF-beta responsiveness. Am J Physiol Lung Cell Mol Physiol 303, L169–L180.
McKenzie AJ, Campbell SL, Howe AK (2011). Protein kinase A activity and anchoring are required for ovarian cancer cell migration and invasion. PLoS One 6, e26552.
McKenzie AJ, Hicks SR, Svec KV, Naughton H, Edmunds ZL, Howe AK (2018). The mechanical microenvironment regulates ovarian cancer cell morphology, migration, and spheroid disaggregation. Sci Rep 8, 7228.
Meyer CJ, Alenghat FJ, Rim P, Fong JH, Fabry B, Ingber DE (2000). Mechanical control of cyclic AMP signalling and gene transcription through integrins. Nat Cell Biol 2, 666–668.
Mostafavi-Pour Z, Askari J, Parkinson S, Parker P, Ng T, Humphries M (2003). Integrin-specific signaling pathways controlling focal adhesion formation and cell migration. J Cell Biol 161, 155–167.
Myers KA, Applegate KT, Danuser G, Fischer RS, Waterman CM (2011). Distinct ECM mechanosensing pathways regulate microtubule dynamics to control endothelial cell branching morphogenesis. J Cell Biol 192, 321–334.
Nagy Z, Wynne K, von Kriegsheim A, Gambaryan S, Smolenski A (2015). Cyclic nucleotide-dependent protein kinases target ARHGAP17 and ARHGEF6 complexes in platelets. J Biol Chem 290, 29974–29983.
Norambuena A, Schwartz MA (2011). Effects of integrin-mediated cell adhesion on plasma membrane lipid raft components and signaling. Mol Biol Cell 22, 3456–3464.
O'Connor KL, Mercurio AM (2001). Protein kinase A regulates Rac and is required for the growth factor-stimulated migration of carcinoma cells. J Biol Chem 276, 47895–47900.
Panzetta V, Fusco S, Netti PA (2019). Cell mechanosensing is regulated by substrate strain energy rather than stiffness. Proc Natl Acad Sci USA 116, 22004–22013.
Parker KK, Brock AL, Brangwynne C, Mannix RJ, Wang N, Ostuni E, Geisse NA, Adams JC, Whitesides GM, Ingber DE (2002). Directional control of lamellipodia extension by constraining cell shape and orienting cell tractional forces. FASEB J 16, 1195–1204.
Pasapera AM, Plotnikov SV, Fischer RS, Case LB, Egelhoff TT, Waterman CM (2015). Rac1-dependent phosphorylation and focal adhesion recruitment of myosin IIA regulates migration and mechanosensing. Curr Biol 25, 175–186.
Pasapera AM, Schneider IC, Rericha E, Schlaepfer DD, Waterman CM (2010). Myosin II activity regulates vinculin recruitment to focal adhesions through FAK-mediated paxillin phosphorylation. J Cell Biol 188, 877–890.
Paulucci-Holthauzen AA, Vergara LA, Bellot LJ, Canton D, Scott JD, O'Connor KL (2009). Spatial distribution of protein kinase A activity during cell migration is mediated by A-kinase anchoring protein AKAP Lbc. J Biol Chem 284, 5956–5967.
Plotnikov SV, Pasapera AM, Sabass B, Waterman CM (2012). Force fluctuations within focal adhesions mediate ECM-rigidity sensing to guide directed cell migration. Cell 151, 1513–1527.
Plotnikov SV, Waterman CM (2013). Guiding cell migration by tugging. Curr Opin Cell Biol 25, 619–626.
Prager-Khoutorsky M, Lichtenstein A, Krishnan R, Rajendran K, Mayo A, Kam Z, Geiger B, Bershadsky AD (2011). Fibroblast polarization is a matrix-rigidity-dependent process controlled by focal adhesion mechanosensing. Nat Cell Biol 13, 1457–1465.
Raslan Z, Naseem KM (2015). Compartmentalisation of cAMP-dependent signalling in blood platelets: the role of lipid rafts and actin polymerisation. Platelets 26, 349–357.
Ringer P, Colo G, Fassler R, Grashoff C (2017). Sensing the mechano-chemical properties of the extracellular matrix. Matrix Biol 64, 6–16.
Riveline D, Zamir E, Balaban NQ, Schwarz US, Ishizaki T, Narumiya S, Kam Z, Geiger B, Bershadsky AD (2001). Focal contacts as mechanosensors: externally applied local mechanical force induces growth of focal contacts by an mDia1-dependent and ROCK-independent mechanism. J Cell Biol 153, 1175–1186.
Robertson J, Jacquemet G, Byron A, Jones MC, Warwood S, Selley JN, Knight D, Humphries JD, Humphries MJ (2015). Defining the phospho-adhesome through the phosphoproteomic analysis of integrin signalling. Nat Commun 6, 6265.
Roca-Cusachs P, Sunyer R, Trepat X (2013). Mechanical guidance of cell migration: lessons from chemotaxis. Curr Opin Cell Biol 25, 543–549.
Rodan GA, Bourret LA, Harvey A, Mensi T (1975). Cyclic AMP and cyclic GMP: mediators of the mechanical effects on bone remodeling. Science 189, 467–469.
Ruppelt A, Mosenden R, Gronholm M, Aandahl EM, Tobin D, Carlson CR, Abrahamsen H, Herberg FW, Carpen O, Tasken K (2007). Inhibition of T cell activation by cyclic adenosine 5'-monophosphate requires lipid raft targeting of protein kinase A type I by the A-kinase anchoring protein ezrin. J Immunol 179, 5159–5168.
Sakamoto T, Limouze J, Combs CA, Straight AF, Sellers JR (2005). Blebbistatin, a myosin II inhibitor, is photoinactivated by blue light. Biochemistry 44, 584–588.
Schiffhauer ES, Robinson DN (2017). Mechanochemical signaling directs cell-shape change. Biophys J 112, 207–214.
Schiller HB, Fassler R (2013). Mechanosensitivity and compositional dynamics of cell–matrix adhesions. EMBO Rep 14, 509–519.
Schwartz MA (2010). Integrins and extracellular matrix in mechanotransduction. Cold Spring Harb Perspect Biol 2, a005066.
Schwartz MA, DeSimone DW (2008). Cell adhesion receptors in mechanotransduction. Curr Opin Cell Biol 20, 551–556.
Scott JD, Dessauer CW, Tasken K (2013). Creating order from chaos: cellular regulation by kinase anchoring. Annu Rev Pharmacol Toxicol 53, 187–210.
Sinha C, Ren A, Arora K, Moon CS, Yarlagadda S, Woodrooffe K, Lin S, Schuetz JD, Ziady AG, Naren AP (2015). PKA and actin play critical roles as downstream effectors in MRP4-mediated regulation of fibroblast migration. Cell Signal 27, 1345–1355.
Skroblin P, Grossmann S, Schafer G, Rosenthal W, Klussmann E (2010). Mechanisms of protein kinase A anchoring. Int Rev Cell Mol Biol 283, 235–330.
Smith FD, Esseltine JL, Nygren PJ, Veesler D, Byrne DP, Vonderach M, Strashnov I, Eyers CE, Eyers PA, Langeberg LK, Scott JD (2017). Local protein kinase A action proceeds through intact holoenzymes. Science 356, 1288–1293.
Storch U, Mederos y Schnitzler M, Gudermann T (2012). G protein-mediated stretch reception. Am J Physiol Heart Circ Physiol 302, H1241–H1249.
Sun X, Fu Y, Gu M, Zhang L, Li D, Li H, Chien S, Shyy JY, Zhu Y (2016). Activation of integrin alpha5 mediated by flow requires its translocation to membrane lipid rafts in vascular endothelial cells. Proc Natl Acad Sci USA 113, 769–774.
Svec KV, Patterson JB, Naim N, Howe AK (2019). Single cell durotaxis assay for assessing mechanical control of cellular movement and related signaling events. J Vis Exp 2019, doi: 10.3791/59995.
Takahashi M, Dillon TJ, Liu C, Kariya Y, Wang Z, Stork PJ (2013). Protein kinase A-dependent phosphorylation of Rap1 regulates its membrane localization and cell migration. J Biol Chem 288, 27712–27723.

Tkachenko E, Sabouri-Ghomi M, Pertz O, Kim C, Gutierrez E, Machacek M, Groisman A, Danuser G, Ginsberg MH (2011). Protein kinase A governs a RhoA-RhoGDI protrusion-retraction pacemaker in migrating cells. Nat Cell Biol 13, 660–667.

Tonucci FM, Almada E, Borini-Etichetti C, Pariani A, Hidalgo F, Rico MJ, Girardini J, Favre C, Goldenring JR, Menacho-Marquez M, Larocca MC (2019). Identification of a CIP4 PKA phosphorylation site involved in the regulation of cancer cell invasiveness and metastasis. Cancer Lett 461, 65–77.

Totsukawa G, Yamakita Y, Yamashiro S, Hartshorne DJ, Sasaki Y, Matsumura F (2000). Distinct roles of ROCK (Rho-kinase) and MLCK in spatial regulation of MLC phosphorylation for assembly of stress fibers and focal adhesions in 3T3 fibroblasts. J Cell Biol 150, 797–806.

Tse JR, Engler AJ (2010). Preparation of hydrogel substrates with tunable mechanical properties. Curr Protoc Cell Biol Chapter 10, Unit 10 16.

Tseng Q, Duchemin-Pelletier E, Deshiere A, Balland M, Guillou H, Filhol O, Thery M (2012). Spatial organization of the extracellular matrix regulates cell-cell junction positioning. Proc Natl Acad Sci USA 109, 1506–1511.

Varkuti BH, Kepiro M, Horvath IA, Vegner L, Rati S, Zsigmond A, Hegyi G, Lenkei Z, Varga M, Malnasi-Csizmadia A (2016). A highly soluble, non-phototoxic, non-fluorescent blebbistatin derivative. Sci Rep 6, 26141.

Vassilieva EV, Gerner-Smidt K, Ivanov AI, Nusrat A (2008). Lipid rafts mediate internalization of beta1-integrin in migrating intestinal epithelial cells. Am J Physiol Gastrointest Liver Physiol 295, G965–G976.

Vicente-Manzanares M, Newell-Litwa K, Bachir AI, Whitmore LA, Horwitz AR (2011). Myosin IIA/IIB restrict adhesive and protrusive signaling to generate front-back polarity in migrating cells. J Cell Biol 193, 381–396.

Wakatsuki T, Wysolmerski RB, Elson EL (2003). Mechanics of cell spreading: role of myosin II. J Cell Sci 116, 1617–1625.

Wang HB, Dembo M, Hanks SK, Wang Y (2001). Focal adhesion kinase is involved in mechanosensing during fibroblast migration. Proc Natl Acad Sci USA 98, 11295–11300.

Wang R, Bi J, Ampah KK, Ba X, Liu W, Zeng X (2013). Lipid rafts control human melanoma cell migration by regulating focal adhesion disassembly. Biochim Biophys Acta 1833, 3195–3205.

Weinberg SH, Mair DB, Lemmon CA (2017). Mechanotransduction dynamics at the cell–matrix interface. Biophys J 112, 1962–1974.

Whittard JD, Akiyama SK (2001). Positive regulation of cell–cell and cell–substrate adhesion by protein kinase A. J Cell Sci 114, 3265–3272.

Wolfenson H, Bershadsky A, Henis YI, Geiger B (2011). Actomyosin-generated tension controls the molecular kinetics of focal adhesions. J Cell Sci 124, 1425–1432.

Yeo MG, Oh HJ, Cho HS, Chun JS, Marcantonio EE, Song WK (2011). Phosphorylation of Ser 21 in Fyn regulates its kinase activity, focal adhesion targeting, and is required for cell migration. J Cell Physiol 226, 236–247.

Zaidel-Bar R, Ballestrem C, Kam Z, Geiger B (2003). Early molecular events in the assembly of matrix adhesions at the leading edge of migrating cells. J Cell Sci 116, 4605–4613.

Zhang D, Ouyang J, Wang N, Zhang Y, Bie J, Zhang Y (2010). Promotion of PDGF-induced endothelial cell migration by phosphorylated VASP depends on PKA anchoring via AKAP. Mol Cell Biochem 335, 1–11.

Zhang X, Jiang G, Cai Y, Monkley SJ, Critchley DR, Sheetz MP (2008). Talin depletion reveals independence of initial cell spreading from integrin activation and traction. Nat Cell Biol 10, 1062–1068.